

3-10-2006

Carrier dynamics in α -Fe₂O₃ (0001) thin films and single crystals probed by femtosecond transient absorption and reflectivity

Alan G. Joly

Joshua R. Williams


Scott A. Chambers

Gang Xiong

Wayne P. Hess

See next page for additional authors

Follow this and additional works at: <https://digitalcommons.cwu.edu/cotsfac>

 Part of the [Physics Commons](#)

Authors

Alan G. Joly, Joshua R. Williams, Scott A. Chambers, Gang Xiong, Wayne P. Hess, and David M. Laman

Carrier dynamics in α -Fe₂O₃ (0001) thin films and single crystals probed by femtosecond transient absorption and reflectivity

Alan G. Joly,^{a)} Joshua R. Williams, Scott A. Chambers, Gang Xiong, and Wayne P. Hess
Pacific Northwest National Laboratory, P.O. Box 999, Richland, Washington 99352

David M. Laman
Central Washington University, Ellensburg, Washington 98926

(Received 1 September 2005; accepted 25 January 2006; published online 10 March 2006)

Femtosecond transient reflectivity and absorption are used to measure the carrier lifetimes in α -Fe₂O₃ thin films and single crystals. The results from the thin films show that initially excited hot electrons relax to the band edge within 300 fs and then recombine with holes or trap within 5 ps. The trapped electrons have a lifetime of hundreds of picoseconds. Transient reflectivity measurements from hematite (α -Fe₂O₃) single crystals show similar but slightly faster dynamics leading to the conclusion that the short carrier lifetimes in these materials are due primarily to trapping to Fe *d-d* states in the band gap. In the hematite single crystal, the transient reflectivity displays oscillations due to the formation of longitudinal acoustic phonons generated following absorption of the ultrashort excitation pulse. © 2006 American Institute of Physics.

[DOI: 10.1063/1.2177426]

INTRODUCTION

Metal oxides provide a diverse class of materials with a wide range of electronic, magnetic, optical, and chemical properties. For instance, while materials such as TiO₂ and Fe₂O₃ are semiconductors, other oxides such as MgO and Al₂O₃ form wide band gap insulators. The inclusion of *d* orbitals and multiple oxidation states can lead to an abundance of interesting surface and bulk properties and can have tremendous impact on processes such as photocatalysis. In particular, iron oxides have long been of interest as heterogeneous catalysts, pigments, gas sensors, magnetic materials, and as components of both terrestrial and extraterrestrial soils. Much of this interest stems from its relatively small band gap (~2.2 eV), good chemical stability, low toxicity, and ease of preparation. α -Fe₂O₃, which occurs naturally as the mineral hematite, has been the interest of a number of studies but has not found widespread use in photoinitiated devices. This is likely due to its low photocurrent quantum efficiency and conductivity resulting from short carrier lifetimes due to electron-hole recombination, rapid electron trapping, and low hole mobilities.

Hematite has the corundum structure with a hexagonal unit cell and octahedrally coordinated Fe³⁺ atoms. The resulting electronic spectra display Fe³⁺ ligand field transitions and multiple Fe³⁺ excitations in the visible and near-uv region of the spectrum.¹ Higher lying ligand-to-metal charge transfer transitions are also observed in the UV region.¹ The band gap at 2.2 eV is likely of Fe³⁺ *d-d* origin and indirect in nature although higher lying direct transitions from the O²⁻ 2*p* valence band orbitals to the conduction band occur above 3 eV.^{1,2} Recent luminescence measurements on nanoparticles of α -Fe₂O₃ demonstrate that excitation at near 3.2 eV

results in an extremely low quantum yield of about 1×10^{-5} , and higher lying direct transitions above 4.9 eV show only a slightly increased quantum yield.³ The lack of significant radiative recombination naturally implies that fast nonradiative processes such as carrier trapping and phonon coupling severely limit the carrier lifetimes in these materials. Indeed, femtosecond transient absorption measurements on both α -Fe₂O₃ and γ -Fe₂O₃ colloidal nanoparticles display extremely fast transient decays of 0.36 and 4.2 ps, as well as a longer 67 ps response.³ The fast decays were attributed to electron-hole recombination mediated by a high density of trap states within the band gap.³ Unfortunately, α -Fe₂O₃ nanoparticles are likely to contain numerous surface defects or trap states and may have complications due to quantum confinement effects making it difficult to understand the dynamics of such a complex system. Thus, it is difficult to assess the relative material merits based on these measurements alone.

Recent advances in nanotechnology have produced hematite as nanocrystalline powders as well as nanoparticles in colloidal solution,^{3,4} and nanorods,⁵ which may be utilized as catalytic materials. Improvements in CO photocatalysis have been observed by using Fe₂O₃ nanoparticles in place of larger-sized Fe₂O₃ materials.⁶ Thus, the ability to engineer materials on the nanoscale dimension could provide pathways to overcome the intrinsic barriers to charge separation in Fe₂O₃. Along this line, recent advances in thin film growth of layered α -Fe₂O₃ and α -Cr₂O₃ have shown noncommutative band offsets, the manifestation of which may be increased charge separation at the interfaces due to an increase in the interfacial dipole.⁷ Recent theoretical work attributes this noncommutative band offset and by extension increased interfacial dipole to the differences between split-metal and oxygen-divided interfaces.⁸ However, initial experimental tests of α -Fe₂O₃/ α -Cr₂O₃ heterostructures demonstrate that α -Cr₂O₃ is able to promote hole-mediated photodecomposi-

^{a)} Author to whom correspondence should be addressed; FAX: 509 376 6066; electronic mail: agjoly@pnl.gov

tion of adsorbed trimethyl acetic acid on its own, and that any effects due to the staggered band alignment are not experimentally observable.⁹ In addition, epitaxially grown thin films offer a controlled, nearly defect-free single-crystal material in which to study the true dynamics following photoexcitation. Comparison to naturally occurring hematite single crystals as well as previous nanoparticle results may then lead to a better understanding of the photoinitiated carrier dynamics. Clearly more work is needed to understand if heterostructures involving iron oxides can overcome some of the obstacles needed to serve as efficient photocatalysts and electrodes. In a first step towards characterizing these multilayer heterostructures, the basic photophysics of α -Fe₂O₃ thin films and single crystals must be characterized and understood. We report experiments utilizing time-resolved transient absorption and reflectivity measurements to understand the charge carrier dynamics in thin film α -Fe₂O₃ and compare the results to bulk single crystal hematite.

EXPERIMENT

Epitaxial films were grown on α -Al₂O₃(0001) substrates by oxygen plasma assisted molecular beam epitaxy (OPAMBE), using a system described in detail elsewhere.¹⁰ Films of α -Fe₂O₃ were typically 1000 Å thick, and were grown on a 100 Å thick α -Cr₂O₃ buffer layer to mitigate the large in-plane lattice mismatch between α -Fe₂O₃ and the α -Al₂O₃ substrate [$\Delta a/a=5.80\%$ and 3.36% for α -Fe₂O₃/ α -Al₂O₃(0001) and α -Cr₂O₃/ α -Al₂O₃(0001), respectively].

Single crystals of (0001) platelet mineralogical hematite samples from “iron-rose-type” crystals were polished on one side with 0.05 μ m Al₂O₃ and mounted for transient reflection experiments at near normal incidence. The natural hematite likely contains some impurities such as Ti at concentrations of less than 1 at. % not found in the thin film samples.

The time-resolved transmission and reflectance measurements were performed using a regeneratively amplified Ti:sapphire laser system. The output pulse at 814 nm and 1 kHz repetition rate was split into excitation and probe beams using a 10% beam splitter. The excitation beam was frequency doubled in a 1 mm beta-barium borate (BBO) crystal to produce the excitation pulse at 407 nm (3.0 eV). The probe beam was sent through a computer-controlled variable delay line and then focused into a cell of water to produce a white-light continuum. The probe photon energy was frequency selected using 10 nm bandpass interference filters and then focused with the pump pulse onto the sample. The reflected and transmitted probe beams were simultaneously monitored using amplified Si photodiodes. The angle of the reflected probe beam was less than 5° from normal incidence. The excitation beam was modulated using an optical chopper and the intensities of the transmitted and reflected beams detected using lock-in amplifiers. In this way, both the transient reflectivity and transmission from the same region of the sample were collected simultaneously. Pump intensities were limited below the damage threshold of the material and estimates of the excited carrier density are in

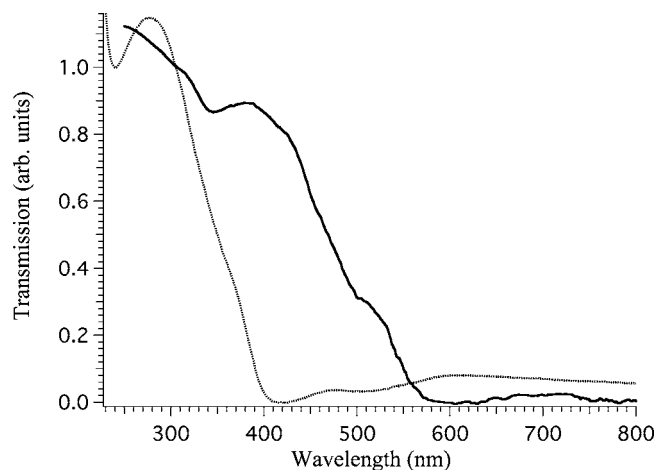


FIG. 1. Transmission as a function of wavelength for a 100 nm Fe₂O₃ thin film grown on a 10 nm Cr₂O₃ buffer layer on a sapphire substrate (solid line) and a 75 nm Cr₂O₃ thin film on a sapphire substrate (dotted line).

excess of $10^{18}/\text{cm}^3$. Experiments were performed multiple times on different regions of the samples and although the relative amplitudes of the different components of the signal sometimes varied, the underlying dynamics were identical. Control experiments were also performed on a 75 nm thick Cr₂O₃ film deposited on sapphire. The Cr₂O₃ thin film produced transient signals at least an order of magnitude smaller than the corresponding transients from α -Fe₂O₃ at all probe wavelengths investigated. The reported results are for parallel pump and probe polarizations, although experiments performed with other polarization combinations produced nearly identical results. The time resolution determined by fitting the rising edge of the transient signals was found to be about 300 fs full width at half maximum (FWHM).

RESULTS AND DISCUSSION

Figure 1 displays a transmission spectrum of a 100 nm Fe₂O₃ thin film prepared on a sapphire substrate with a 10 nm Cr₂O₃ buffer layer. A transmission spectrum of a pure 75 nm thick Cr₂O₃ film on a sapphire substrate is also shown for comparison. For both Fe₂O₃ and Cr₂O₃, the reflectivity differences over the wavelength region shown are on the order of 10% (Refs. 4 and 11) so that the observed transmission spectrum is fairly indicative of the absorption spectrum over this region. The onset of absorption for the Fe₂O₃ thin film at 560 nm (2.2 eV) agrees well with previous measurements for the optical band gap of Fe₂O₃.¹² The weak band centered at about 700 nm (1.8 eV) is thought to originate from ligand field *d-d* transitions.^{1,2} From Fig. 1 it is clear that excitation at 407 nm (3.0 eV) results in efficient excitation of the Fe₂O₃ layer while achieving negligible excitation in the Cr₂O₃ layer or sapphire substrate.

Figure 2 shows the time-resolved reflectance measurements (dotted lines) from the 100 nm Fe₂O₃ thin film using probe wavelengths of 460 and 500 nm (2.7 and 2.5 eV). Also shown in Fig. 2 is the corresponding time-resolved transmission measurements (solid lines), recorded simultaneously with the transient reflectivity. Figure 3 shows the corresponding data observed using probe wavelengths of 560 and 680 nm (2.2 and 1.8 eV). Time-resolved transient reflectivity

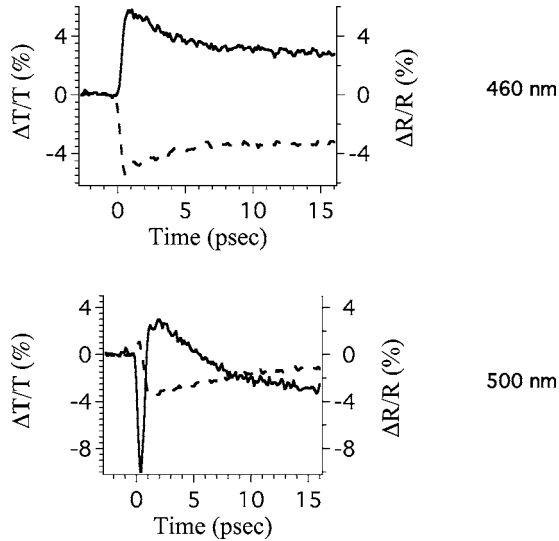


FIG. 2. Femtosecond transient reflectivity (dotted lines) and absorption (solid lines) following excitation at 407 nm (3.0 eV) from a 100 nm thick Fe_2O_3 film at probe wavelengths of 460 nm (2.7 eV) and 500 nm (2.5 eV).

and absorption experiments measure the changes in the real and imaginary parts of the refractive index following photoexcitation. The changes in the real and imaginary parts of the refractive index primarily reflect the excited carrier dynamics. The data shown in Figs. 2 and 3 are readily analyzed assuming that the photoexcited carrier concentration decays exponentially following photoexcitation.

There are a number of interesting features displayed by the transient reflectivity and transmission curves. First, different probe wavelengths show different polarity signals and some, notably 500 nm, show bipolar transients. Similar bipolar transients are observed using probe wavelengths of 480 and 520 nm (data not shown). Second, there is an initial pulse-width-limited change in the signal at all wavelengths. This initial rise is followed by a fast pulse-width-limited decay at probe energies at and below the band gap or by a 3.0 ps decay at probe energies above the band gap. Third, for

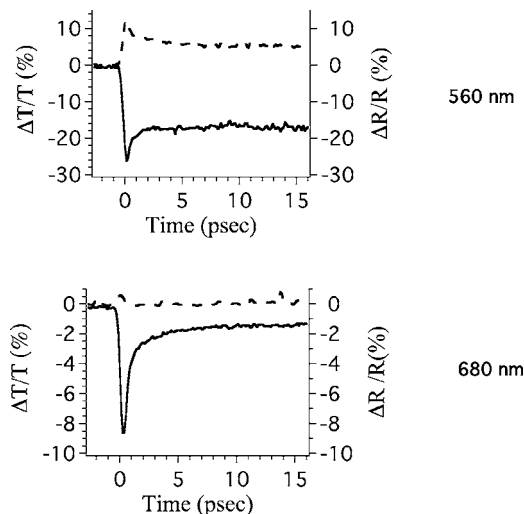


FIG. 3. Femtosecond transient reflectivity (dotted lines) and absorption (solid lines) following excitation at 407 nm (3.0 eV) from a 100 nm thick Fe_2O_3 film at probe wavelengths of 560 nm (2.2 eV) and 680 nm (1.8 eV).

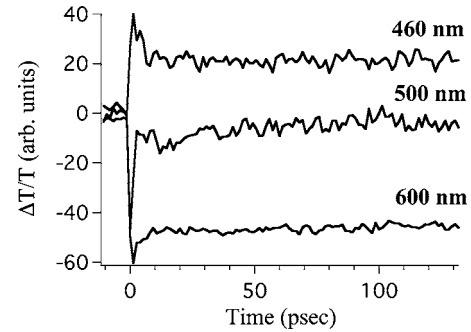


FIG. 4. Longer time femtosecond transient transmission data following excitation at 407 nm (3.0 eV) for a 100 nm thick Fe_2O_3 film at probe wavelengths of 460, 500, and 600 nm.

all wavelengths, there exists a dc offset that is present following the decay of the initial faster transients. Figure 4 displays the longer time scans which show that this dc component shows dynamics on the hundreds of picosecond time scales and beyond. Thus, the dynamics following photoexcitation in the hematite thin film display three time scales ranging from a few hundred femtoseconds to hundreds of picoseconds.

Figure 5 depicts the sign and magnitude of the changes in transmission, reflectivity, and absorption of the shortest time scale (300 fs) feature. Figure 5 clearly shows that the largest signal changes are observed at probe energies near the band gap. These changes can be attributed to hot conduction band electron relaxation resulting in band filling and band gap shrinkage as the electrons relax to the band edge. These effects occur on the hundreds of femtosecond time scales and are expected to be manifest largely at probe regions at or near the band gap.¹³ The polarity of the signal also changes signs near the band gap, consistent with calculations.¹³ Therefore, the initial fast transients may be assigned to hot electron relaxation, band filling, and band gap shrinkage following photoexcitation. The interesting bipolar transients

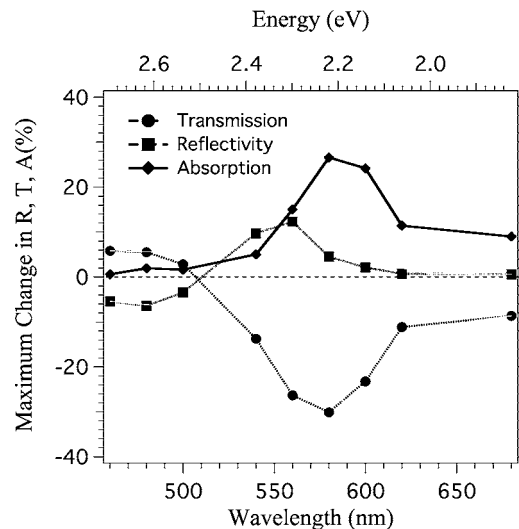


FIG. 5. Maximum change in reflectivity (squares), transmission (circles), and absorption (diamonds) for a 100 nm thick Fe_2O_3 film at different probe energies above and below the band gap at 2.2 eV. The largest changes in both reflectivity and absorption occur near the band gap energy as expected for band filling and band gap shrinkage.

may represent the competition between these effects as they may have opposite polarity at certain probe wavelengths.¹³ In addition, both band gap shrinkage and band filling contributions evolve as the nascent carriers cool to the band edge. These effects occur within the pulse width (300 fs) as expected.

Because of the differences in effective masses of the photoexcited electrons and holes, electron relaxation dynamics are expected to occur on faster time scales relative to hole dynamics. Indeed, following the initial pulse-width-limited rise, the red probe region shows fast (~ 300 fs) pulse-width-limited decays whereas the blue probe region shows slower, 3.0 ps transients. As mentioned above, the red probe region is likely to probe the excited electron absorption, thus the fast pulse width decay is indicative of hot conduction band electron relaxation. Probe wavelengths significantly above the band gap can probe different dynamics. The initial pump pulse at 407 nm (3.0 eV) creates both excited electrons and holes. Initial excitation at 407 nm bleaches the absorption spectrum at and near the excitation wavelength. Therefore the hole recovery time can be measured by monitoring this region of the spectrum. Indeed, recent femtosecond transient absorption experiments on GaAs demonstrate that probe wavelengths significantly above the band gap probe hole recovery dynamics.^{14,15} This suggests that hole recovery occurs, at least partially, on the 3.0 ps time scale.

The electron dynamics probed between the band edge (560 nm) and the far red region of the spectrum also show dynamics that can be fit to a 2.9 ps lifetime. Thus, the time scale for hole recovery and electron relaxation match, suggesting that this is the time scale for electron-hole recombination. This time scale would be consistent with the observed low quantum yield. Trapping likely occurs to a large fraction of the carriers, however. The trapped electrons then lead to the dc component present in the 560–680 nm region of the spectrum. The corresponding dc component in the blue region of the spectrum signifies the fact that these trapped electrons cannot immediately recombine with the holes, thus the hole recovery time shows a longer time component as well. The nature of these trap states is not clear. α -Fe₂O₃ has low-lying electronic states below the conduction band edge¹ and oxygen-deficient Fe³⁺ defect sites,¹⁶ both of which may trap the photoexcited electrons. From our measurements, these trapped carriers do not relax for hundreds of picoseconds to nanoseconds. This is noticeably longer than the carrier recovery time observed in α -Fe₂O₃ nanoparticles where trapped electrons were observed to decay with a 67 ps lifetime.³ This longer trapped electron relaxation time for the thin films may be due to weaker electron-phonon coupling in these materials.

It is interesting to compare the carrier dynamics in thin films to results from single crystal (naturally occurring) hematite as the thin films are relatively thick and should behave similarly to bulk material. Figure 6 displays the time-resolved reflectivity measurements from a ~ 500 μm thick hematite single crystal following excitation at 407 nm (3.0 eV) for probe wavelengths of 460, 500, 560, and 620 nm. Transmission experiments could not be performed simultaneously due to probe beam absorption within the bulk

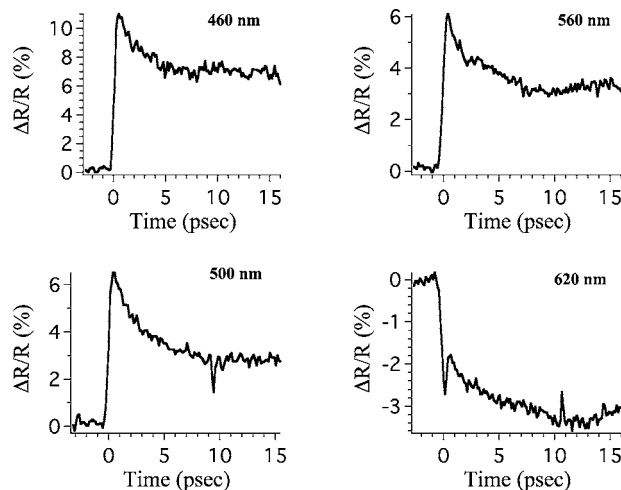


FIG. 6. Femtosecond transient reflectivity following 407 nm (3.0 eV) excitation from a single crystal of hematite using probe wavelengths of 500, 560, 620, and 680 nm.

of the sample. The transient reflectivity data have both similarities to and differences from the hematite thin film data. First of all, the polarity of the reflectivity changes is positive (increased transient reflectivity) at higher probe energies, and undergo a polarity reversal near the band gap such that at probe energies below the band gap the transient reflectivity changes are negative (decreased transient reflectivity). This is exactly opposite to the polarity of the responses from the thin film, although the reversal at the band gap is identical. Second, the transient reflectivity at 460 nm shows a fast initial rise followed by a slower, 2.0 ps recovery to a constant offset, similar to the results from the thin film although the dynamics appear slightly faster. The transient reflectivity signals at probe energies near the band gap show a fast initial rise followed by a pulse-width-limited sharp decrease and then a subsequent slower 2.5 ps decay to a nonzero base line. This is also similar to the results from the thin film although there is no evidence of bipolar transients at wavelengths slightly above the band gap. The transient reflectivity signals at red probe energies below the band gap show the fast pulse-width-limited rise and decay followed by an exponential growth feature with a time constant of 5 ps. This is in marked difference to the results from the thin films. This may be due to the different natures of the numerous defect states within the single crystal. These trap states may have much stronger absorptions in the red, thus showing up strongly in the transient response compared to the thin films.

The photodynamics of the naturally occurring single crystal and the epitaxially grown single crystal are similar. The epitaxially grown film is likely to have significantly fewer defects as well as impurities, both of which would introduce midgap states responsible for photoelectron trapping. Both materials do, however, possess Fe *d-d* transitions within the band gap. The transient reflectivity results indicate that in the hematite single crystal, the carrier lifetime is slightly shorter and that there are increased effects of trapping in the red probe region. Therefore, epitaxially grown films likely have improved qualities relative to the naturally occurring single crystals. However, even in the thin film

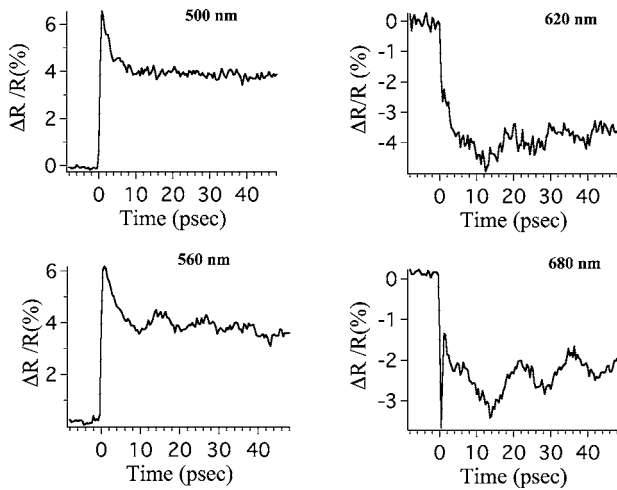


FIG. 7. Longer time femtosecond transient reflectivity following 407 nm (3.0 eV) excitation from a single crystal of hematite using probe wavelengths of 500, 620, and 680 nm. The oscillations in the reflectivity have a frequency of 68 GHz and appear only at probe energies at or below the band gap.

samples, the carrier lifetime is extremely short. It is likely that the fast trapping of the excited electrons is due to the existence of *d-d* states within the band gap and is not a consequence of the impurities or defects in most hematite samples. This coupled with strong electron-phonon coupling likely limits the carrier lifetimes and hence the utility of these materials in photoinitiated devices where long carrier lifetimes are essential.

Figure 7 displays the transient reflectivity response of the hematite single crystal on a longer time scale. There are two noticeable features in the response, the first is the persistence of the offset component at all wavelengths similar to the thin film data. Once more this can be assigned to trapped electron absorption. The second is the appearance of low-frequency oscillations at all probe wavelengths at or below the band gap. The frequency of this oscillation is about 68 GHz, indicative of a longitudinal acoustic phonon. Optical excitation of longitudinal acoustic phonons with short light pulses has been observed in bulk GaN and AlGaN thin films,¹⁷ as well as a variety of quantum wells and heterostructures.^{18–21} The generation of the acoustic phonon is a result of an elastic deformation caused by local heating following strong absorption of an ultrashort pump pulse.^{22,23} The absorption of the pump pulse initially creates hot electrons and holes that ultimately lose their energy through collisions with the lattice. This results in an elastic deformation that launches a strain pulse from the front region of the material. This strain pulse propagates away from the front of the sample with a velocity determined by the speed of sound in the material. The delayed probe pulse then experiences regions of compression and rarefaction over the probe pulse penetration length and these regions propagate through the sample at the sound velocity. The reflected probe can be considered as the interference of light reflected from both the front surface region and the moving compressional wave. This leads to oscillations in the reflectivity and transmission of the sample provided that the probe pulse penetration depth is larger than the deformation pulse width.

The width of the strain pulse corresponds to about twice the optical penetration depth, determined by the absorption coefficient α .^{22,23} For hematite using an excitation wavelength of about 400 nm, the optical penetration depth is roughly 100 nm leading to a deformation pulse width of about 200 nm. Probe pulses at different wavelengths experience varying amounts of modulation because of the different penetration depths of the probe at different wavelengths. At energies above the band gap, the probe pulse penetration depth is similar to the deformation pulse width and very little modulation is observed because the deformation appears almost uniform over this distance. At probe energies below the band gap, the probe penetration depth is greater than the sample thickness, thus interference between the reflected waves from the front surface and the elastic deformation pulse can be observed as oscillations in the total reflected probe intensity. This is likely why the modulations in the signal are not observed at probe wavelengths above the band gap in the hematite single crystal.

From the oscillation period, the velocity of sound (v_s) can be calculated according to²²

$$v_s = \frac{\lambda}{2nt},$$

where t is the modulation period and λ is the probe wavelength. This leads to a value of about 6×10^3 m/s in the hematite single crystal. In the case of the thin film, the optical penetration depth is about the same length as the thickness of the sample. The associated strain pulse is actually broader than the film thickness, therefore the probe experiences the strain as a nearly homogeneous deformation and no oscillations in the reflected intensity are observed. Similarly, femtosecond transient absorption experiments on α -Fe₂O₃ nanoparticles using red probe wavelengths did not observe such oscillations³ presumably because the width of the elastic deformation is significantly larger than the particle size.

In summary, the transient response of a 100 nm α -Fe₂O₃ thin film may be described by the following scenario. Initially, excited electrons relax to the conduction band edge within 300 fs. Recombination with holes and trapping of electrons occurs in approximately 3 ps. The resulting trap states exist for hundreds of picoseconds or longer. Measurements on single crystal α -Fe₂O₃ demonstrate slightly faster dynamics compared to the thin film but with a greater manifestation of electron trapping. This may be due to the single crystal containing a larger number of more varied trap sites. While the epitaxially grown thin films display improved qualities relative to the naturally occurring Fe₂O₃ single crystals, the carrier lifetimes are not significantly increased. This points to carrier trapping by midgap Fe *d-d* states as the dominant trapping mechanism. Longer time scans from the hematite single crystal reveal coherent oscillations not observed in the thin film measurements. These oscillations derive from longitudinal acoustic phonons launched following absorption of the pump pulse.

ACKNOWLEDGMENTS

The authors thank Ann Chiaramonte, Peter Stair, and Laurie Marks for providing the single crystal hematite sample. This work was funded by the Nanoscience Engineering and Technology (NSET) program of the U.S. Department of Energy's Office of Science, Division of Chemical Sciences. Part of the research described in this paper was performed at the W.R. Wiley Environmental Molecular Sciences Laboratory, a national scientific user facility sponsored by the Department of Energy's Office of Biological and Environmental Research and located at the Pacific Northwest National Laboratory (PNNL). PNNL is operated by Battelle for the U.S. Department of Energy under Contract No. DE-AC06-76RLO1830.

¹D. M. Sherman and T. D. Waite, *Am. Mineral.* **70**, 1262 (1985).

²L. A. Marusak, R. Messier, and W. B. White, *J. Phys. Chem. Solids* **41**, 981 (1980).

³N. J. Cherepy, D. B. Liston, J. A. Lovejoy, H. Deng, and J. Z. Zhang, *J. Phys. Chem. B* **102**, 770 (1998).

⁴N. H. G. Penners and L. K. Koopal, *Colloids Surf.* **19**, 337 (1986).

⁵Y. Xiong, Z. Li, X. Li, B. Hu, and Y. Xie, *Inorg. Chem.* **43**, 6540 (2004).

⁶P. Li, D. E. Miser, S. Rabiei, R. T. Yadav, and M. R. Hajaligol, *Appl. Catal., B* **43**, 151 (2003).

⁷S. A. Chambers, Y. Liang, and Y. Gao, *Phys. Rev. B* **61**, 13223 (2000).

⁸J. E. Jaffe, M. Dupuis, and M. Gutowski, *Phys. Rev. B* **69**, 205106 (2004).

⁹S. A. Chambers, J. R. Williams, M. A. Henderson, A. G. Joly, M. Varela, and S. J. Pennycook, *Surf. Sci.* **587**, L197 (2005).

¹⁰S. A. Chambers, *Surf. Sci. Rep.* **39**, 105 (2000).

¹¹V. Teixeira *et al.*, *Thin Solid Films* **392**, 320 (2001).

¹²S. Mohanty and J. Ghose, *J. Phys. Chem. Solids* **53**, 81 (1992).

¹³B. R. Bennett, R. A. Soref, and J. A. Del Alamo, *IEEE J. Quantum Electron.* **26**, 113 (1990).

¹⁴R. Tommasi, P. Langot, and F. Vallee, *Appl. Phys. Lett.* **66**, 1361 (1995).

¹⁵A. Leitenstorfer, C. Furst, A. Laubereau, W. Kaiser, G. Trankle, and G. Weimann, *Phys. Rev. Lett.* **76**, 1545 (1996).

¹⁶C. Leygraf, M. Hendewerk, and G. Somorjai, *J. Solid State Chem.* **48**, 357 (1983).

¹⁷M. Wraback, H. Shen, A. V. Sampath, C. J. Collins, G. A. Garrett, and W. L. Sarney, *Phys. Status Solidi A* **202**, 790 (2005).

¹⁸U. Ozgur, C.-W. Lee, and H. O. Everitt, *Phys. Rev. Lett.* **86**, 5604 (2001).

¹⁹E. Makarona, B. Daly, J.-S. Im, H. Maris, A. Nurmikko, and J. Han, *Appl. Phys. Lett.* **81**, 2791 (2002).

²⁰C.-K. Sun, J.-C. Liang, and X.-Y. Yu, *Phys. Rev. Lett.* **84**, 179 (2000).

²¹J. S. Yahng, Y. D. Jho, K. J. Yee, E. Oh, J. C. Woo, D. S. Kim, G. D. Sanders, and C. J. Stanton, *Appl. Phys. Lett.* **80**, 4723 (2002).

²²C. Thomsen, H. T. Grahn, H. J. Maris, and J. Tauc, *Phys. Rev. B* **34**, 4129 (1986).

²³H. T. Grahn, H. J. Maris, and J. Tauc, *IEEE J. Quantum Electron.* **25**, 2562 (1989).